Astron. Astrophys. 319, 578–588 (1997)

ASTRONOMY AND ASTROPHYSICS

Constraints on mass loss from dMe stars: theory and observations

G.H.J. van den Oord[1] **and J.G. Doyle**[2]

[1] Sterrenkundig Instituut, P.O. Box 80.000, 3508 TA Utrecht, The Netherlands
[2] Armagh Observatory, Armagh BT61 9DG, Northern Ireland

Received 14 March 1996 / Accepted 21 August 1996

Abstract. We show that the flux distribution of a wind from a cool star differs considerably from what is predicted by the theory for mass loss from hot stars. The differences are caused by the facts that 1) the mass loss rates are lower, resulting in smaller optical depths in the wind, and 2) for winds from cool stars the temperature of the wind is higher than the temperature of the star while for winds from hot stars the reverse holds. These differences result in substantial modifications of the flux distribution and imply that care must be exercised when applying the flux predictions by e.g. Wright and Barlow (1975) to winds from cool stars. By using observational constraints we show that the mass loss from cool dwarf stars equals at most 10^{-12} $M_\odot$/yr. This is a factor hundred lower than previous estimates. At this rate the mass loss from dMe stars is of little importance for the enrichment of the interstellar medium. By solving the radiative transfer equations for stellar winds from dMe stars, we show that the inferred power-law flux distributions, based on radio, *JCMT* and *IRAS* data, cannot be reconciled with the flux distributions from a stellar wind of 10^{-10} $M_\odot$/yr as was previously assumed. The maximum allowable mass loss rate is at most a few times 10^{-12} $M_\odot$/yr which implies that the fluxes observed with *JCMT*, *IRAS*, and in the future with *ISO*, require a different interpretation than free-free emission from a stellar wind.

Key words: stars: late-type – stars: mass-loss –ISM: general – infrared: stars – radio continuum: stars – ultraviolet: stars

1. Introduction

Over the past decade some circumstantial evidence has been obtained that cool dwarf stars may be loosing mass at considerably higher rates than the Sun. The first evidence was found in a UV spectrum of the detached binary V471 Tau (Mullan et al., 1989). This system consists of a white dwarf and a K2V star. Discrete absorption features in the UV continuum of the dwarf could be identified as mass ejections from the K2V star. The temperature of the ejecta was $\lesssim 2\ 10^4$ K and the total mass loss rate caused by the ejecta was estimated to be a few times 10^{-11} $M_\odot$/yr. Houdebine et al. (1990) obtained optical spectra during a flare event on the dMe star AD Leo. It was found that a coronal mass ejection took place during the flare. Based on the flare frequency and depending on the temperature of the ejecta these authors argued that the total flare-related mass loss is the range $2.7\ 10^{-13} - 4.4\ 10^{-10}$ $M_\odot$/yr.

Doyle and Mathioudakis (1991) published the first tentative (2σ) detections of two dMe stars at wavelengths of 1.1 and 2 mm obtained with the *JCMT*. The authors pointed out that the observed fluxes indicate the presence of excess emission at these wavelengths above the black-body emission from the star.

Mullan et al. (1992, hereafter MDRM) pointed out that the combination of radio, *JCMT* and *IRAS* data is indicative of the presence of a power-law flux distribution $F_\nu \sim \nu^\alpha$ with $\alpha \approx 0.7-1$ in the radio – IR range. In Fig. 1 we have reproduced the data on which MDRM based their conclusions. Such power-law distributions are commonly found in the spectra of early type stars undergoing mass loss at rates of $10^{-5} - 10^{-8}$ $M_\odot$/yr (Wright and Barlow, 1975, Lamers and Waters, 1984). By applying the expressions for the expected flux from a mass loosing star, as derived for winds from hot stars, MDRM concluded that certain dMe stars undergo mass loss of rates of a few times 10^{-10} $M_\odot$/yr. This would have profound implications for the mass balance in the interstellar medium. MDRM estimate the total number of M dwarfs in the galactic disk to exceed 10^{11}. The total mass supply to the interstellar medium from the winds of M dwarfs could then amount to 10 $M_\odot$/yr. This value is twenty times higher than the mass supply from the 'normal' donors: OB stars, planetary nebula etc.. In this way M stars could play an important role in the enrichment of the interstellar medium.

There are two important assumptions in the work by MDRM. Firstly, it is assumed that the radio, mm and infrared fluxes are caused by the presence of a stellar wind. Secondly, it is assumed that mass loss rates of 10^{-10} $M_\odot$/yr do result in a power-law flux distribution. The first assumption has important consequences for the interpretation of *ISO* data. The evidence for a wind emission is however scant if one looks at the data. The *IRAS* fluxes at 12μm and 25μm are in reasonable agreement with what is expected from the stellar Planck function. The

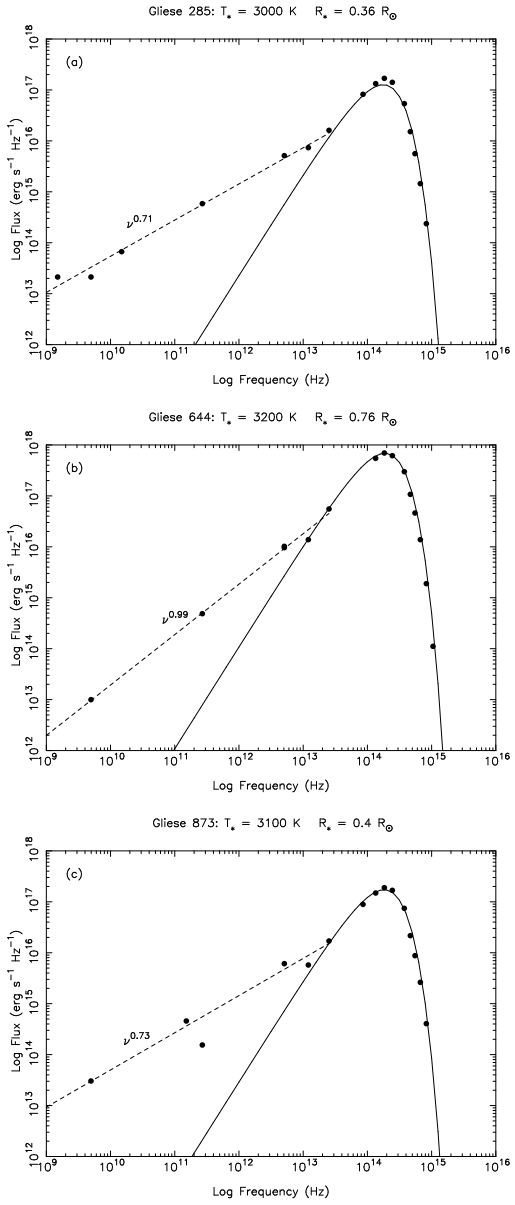

Fig. 1a–c. Reproduction of the data on which MDRM based their estimates for the mass loss rates for dMe stars. The power-law approximations run between the radio data and the *IRAS* data. The data near $\log \nu = 11$ are from the *JCMT*. The objects shown are **a** Gliese 285 = YZ CMi, **b** Gliese 644 = Wolf 630 and **c** Gliese 873 = EV Lac.

excess emission is only present at 60μm and 100μm but these data points are very uncertain due to cirrus or extended source sizes. The *JCMT* data points are near the detection thresh-hold of the bolometric instrument used on the *JCMT* at that time, resulting in less than 3σ detections. The radio emission from dMe stars is commonly interpreted as gyro-synchrotron emission from non-thermal particles or coherent emission and not as free-free emission. The observed variability, the polarization and the required emission measure argue against a wind interpretation. Concerning the second assumption it must be noted that the derived mass loss rates for the dMe stars are factors $10^2 - 10^5$ smaller than those of hot stars. This leads to a decrease of the optical depth in the wind and, as we will show, a modification of the spectrum. A second important difference is that for the winds from hot stars the temperature of the wind is in general lower than the temperature of the star while for cool M dwarfs the reverse holds. This leads to a substantial modification of the flux distribution compared to the distributions found for hot stars.

Because of the importance of mass loss from M dwarfs for the mass balance in the interstellar medium, and because of the importance for the interpretation of *ISO* data we have reanalyzed the data presented by MDRM. Instead of applying the expressions for winds from hot stars we have solved the radiative transfer problem for winds near cool stars. We show that winds from cool stars do not result in a power-law distribution in the radio – IR frequency range. Furthermore we show, by using observational constraints, that the mass loss from the dMe stars cannot be higher than a few times 10^{-12} $M_\odot$/yr.

When this work was completed Lim and White (1996) published independently similar constraints for the mass loss from dMe stars. These authors report an upper limit of 10 mJy at 3.5 mm for YZ CMi obtained with the *BIMA* array. The detection by MDRM of a flux of 13.2 ± 6 mJy at 1.1 mm can be reconciled with the *BIMA* result by noting that the detection at 1.1 mm was only at a 2σ level. Lim and White base their constraints on the fact that the nonthermal radio emission from dMe stars must not be absorbed by a stellar wind, a point we also address in this paper. In this paper we take however into account the ionization state of the wind which permits us to pose constraints on the mass loss rate for a range of wind temperatures. Also we show that the expressions for the flux from a wind, as derived by e.g. Wright and Barlow (1975), cannot be applied directly when the mass loss rate is low and the wind temperature exceeds the temperature of the star.

The outline of the paper is as follows. In Sect. 2 we derived the basic expressions for the free-free emission from a wind taking the ionization balance into account. Also we present effective gaunt factors as follow from a self-consistent treatment of the ionization balance. In Sect. 3 we apply the resulting expressions to the flux distributions discussed by MDRM. Additional observational constraints for the mass loss from dMe stars are discussed in Sect. 4. Our conclusions are presented in Sect. 5.

2. Free-free emission from a wind

For a spherically symmetric wind the equation for mass conservation reads

$$\dot{M} = 4\pi r^2 \rho(r) v(r) = 4\pi r^2 v(r) \mu m_{\rm H} n_{\rm i}(r) \quad (1)$$

where $\dot{M}$ is the mass loss rate, ρ is the mass density, v is the wind velocity, $m_{\rm H}$ is the hydrogen mass, $n_{\rm i}$ is the ion density and μ is the mean atomic weight *per ion*. Because the observed emission originates from the ionized gas component in the wind it is necessary to consider the ionization balance in the wind. Let $n_{\rm e}$ be the electron density, $n_{\rm Z,z}$ the ion density of the ions from the element with atomic number Z and with a charge z, $n_{\rm Z}$

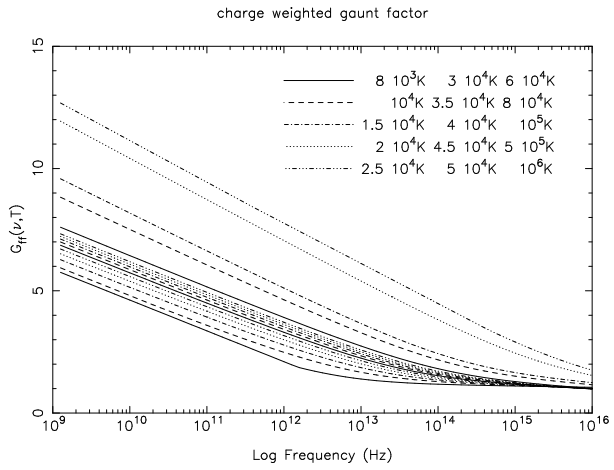

Fig. 2. Gaunt factors, as follow from Eq. (6), as a function of the frequency and for fifteen values of the temperature. Higher curves correspond to higher temperatures.

the total density of neutrals and ions of the element with atomic number Z and $A_{\rm Z} = n_{\rm Z}/n_{\rm H}$ the element abundance. Note that $n_{\rm H} = n({\rm H\ I}) + n({\rm H\ II})$. The electron density is given by

$$n_{\rm e} = \sum_{\rm Z,z} n_{\rm Z,z} z = n_{\rm H} \sum_{\rm Z,z} A_{\rm Z} \frac{n_{\rm Z,z}}{n_{\rm Z}} z \equiv n_{\rm H} S_{\rm e} \qquad (2)$$

while the ion density is given by

$$n_{\rm i} = \sum_{\rm Z,z} n_{\rm Z,z} = n_{\rm H} \sum_{\rm Z,z} A_{\rm Z} \frac{n_{\rm Z,z}}{n_{\rm Z}} \equiv n_{\rm H} S_{\rm i} \ . \qquad (3)$$

The average number of electrons per ion is given by $n_{\rm e}/n_{\rm i} = S_{\rm e}/S_{\rm i} \equiv \gamma$ and the mean atomic mass per ion is given by

$$\mu = \frac{\rho}{m_{\rm H} n_{\rm i}} = \frac{1}{S_{\rm i}} \sum_{\rm Z} A_{\rm Z} \frac{m_{\rm Z}}{m_{\rm H}} \ . \qquad (4)$$

The fraction of neutral hydrogen is given by $\zeta \equiv n({\rm H\ I})/n_{\rm H}$.

Since there is no information available from observations concerning the ionization balance in the wind, the most plausible assumption one can make is that, after an initial acceleration of the wind, the ionization balance is frozen-in due to the rapid decrease of the density. The ionization balance in the wind then reflects the ionization balance at the base of the wind which is determined by collisional ionization equilibrium. We determined the values of $S_{\rm e}$, $S_{\rm i}$, γ, μ and ζ using the ionization balance by Arnaud and Raymond (1992) for iron and by Arnaud and Rothenflug (1985) for the other elements. Solar photospheric abundances were assumed (Anders and Grevesse, 1989). The results are presented in Table 1 for a number of wind temperatures in the range $8000 - 10^6$ K.

The linear free-free absorption coefficient is given by (Allen, 1973)

$$\kappa(\nu,T) = 3.692\ 10^8 \left\{1 - \exp\left(\frac{-h\nu}{kT}\right)\right\} T^{-1/2} \nu^{-2} \times n_{\rm e} \sum_{\rm Z,z} n_{\rm Z,z} z^2 g_{\rm ff}(Z,z,\nu,T) \ . \qquad (5)$$

Table 1. Values for $S_{\rm e} = n_{\rm e}/n_{\rm H}$, $S_{\rm i} = n_{\rm i}/n_{\rm H}$, $\mu = \rho/(m_{\rm H} n_{\rm i})$ and $\zeta = n({\rm H\ I})/n_{\rm H}$ as follow from collisional ionization equilibrium for a number of temperatures. $\overline{G_{\rm ff,R}}$ is the gaunt factor at frequency $10^{9.7}$ Hz.

T(K)	$S_{\rm e}$	$S_{\rm i}$	μ	ζ	$\overline{G_{\rm ff,R}}$
8000	$4\ 10^{-7}$	$4\ 10^{-7}$	$3.528\ 10^6$	1	4.9986
10000	$3\ 10^{-3}$	$3\ 10^{-3}$	466.3	0.997	5.1827
15000	0.419	0.419	3.369	0.582	5.5173
20000	0.935	0.935	1.508	$6.66\ 10^{-2}$	5.7644
25000	1.004	1.004	1.405	$1.09\ 10^{-2}$	5.9574
30000	1.053	1.053	1.340	$3.09\ 10^{-3}$	6.1103
35000	1.085	1.085	1.300	$1.23\ 10^{-3}$	6.2415
40000	1.094	1.094	1.289	$5.98\ 10^{-4}$	6.3592
45000	1.097	1.097	1.286	$3.36\ 10^{-4}$	6.4662
50000	1.099	1.098	1.285	$2.08\ 10^{-4}$	6.5693
60000	1.105	1.099	1.284	$9.81\ 10^{-5}$	6.8255
80000	1.155	1.099	1.283	$3.50\ 10^{-5}$	7.9481
10^5	1.181	1.099	1.283	$2.17\ 10^{-5}$	8.6460
$5\ 10^5$	1.203	1.099	1.283	$6.50\ 10^{-7}$	10.923
10^6	1.203	1.099	1.283	$2.53\ 10^{-7}$	11.6569

The second part of this expression can be written as $\gamma n_{\rm i}^2 \overline{G_{\rm ff}}(\nu,T)$ with

$$\overline{G_{\rm ff}}(\nu,T) = \frac{\sum_{\rm Z,z} n_{\rm Z,z} z^2 g_{\rm ff}(Z,z,\nu,T)}{\sum_{\rm Z,z} n_{\rm Z,z}} \ . \qquad (6)$$

For calculating the gaunt factors we followed the procedure outlined by Waters and Lamers (1984) with the exception that Lamers and Waters write $\overline{G_{\rm ff}} = \overline{z^2} g(\nu,T)$ with $\overline{z^2}$ the mean value of the squared atomic charge. In our case separating out $\overline{z^2}$ would be impractical given the form of Eq. (6). For low values of $h\nu/kT$ we use the expression for the gaunt factor given by Allen (1973) but with the correction discussed by Leitherer and Robert (1991). For high values of $h\nu/kT$ we use the expression by Mewe et al. (1986) (see also Gronenschild and Mewe, 1978). In practice we took the maximum value for $\overline{G_{\rm ff}}$, at a given temperature and frequency, which resulted from these approximations. The results are shown in Fig. 2.

By introducing the dimensionless parameters $x = r/R_*$ and $w(x) = v(r)/v_\infty$, the absorption coefficient can be written as

$$\kappa(\nu,x) = X_* X_\nu \left\{R_* w^2(x) x^4\right\}^{-1} \qquad (7)$$

with

$$X_* = 3.692\ 10^8 \frac{h}{k} \left(\frac{\dot{M}}{4\pi m_{\rm H} v_\infty}\right)^2 T^{-3/2} R_*^{-3} \frac{\gamma}{\mu^2} \qquad (8)$$

and

$$X_\nu = \frac{1 - \exp(-h\nu/kT)}{h\nu/kT} \nu^{-2}\ \overline{G_{\rm ff}} \ . \qquad (9)$$

The constant X_* is independent of the frequency.

Table 2. Expressions for: the optical depth at impact parameter q (see Eqs. (10) and (11)), the emission measure EM of the visible part of a isothermal stellar wind, the neutral hydrogen column density $N_{\rm H}$, the effective radius $r_{\rm eff}$ and the effective optical depth $\tau_{\rm eff}$.

Optical depths as function of impact parameter q:

$q = 0$ $\quad \tau_{\max}(q) = \frac{1}{3} X_* X_\nu \left[\frac{3}{2\beta+3} x_1^{2\beta} \left(1 - x_1^{-2\beta-3}\right) + x_1^{-3} \right] \equiv \frac{1}{3} X_* X_\nu H(x_1, \beta)$

$0 < q \leq 1$ $\quad \tau_{\max}(q) = X_* X_\nu \left[\frac{1}{2} \left(\frac{x_1}{q}\right)^{2\beta} q^{-3} \left\{ B_{q^2}(\beta + \frac{3}{2}, \frac{1}{2}) - B_{q^2/x_1^2}(\beta + \frac{3}{2}, \frac{1}{2}) \right\} + \frac{1}{2} q^{-3} B_{q^2/x_1^2}(\frac{3}{2}, \frac{1}{2}) \right]$

$1 < q < x_1$ $\quad \tau_{\max}(q) = X_* X_\nu \left[\left(\frac{x_1}{q}\right)^{2\beta} q^{-3} \left\{ B(\beta + \frac{3}{2}, \frac{1}{2}) - B_{q^2/x_1^2}(\beta + \frac{3}{2}, \frac{1}{2}) \right\} + q^{-3} B_{q^2/x_1^2}(\frac{3}{2}, \frac{1}{2}) \right]$

$q \geq x_1$ $\quad \tau_{\max}(q) = \frac{1}{2} \pi X_* X_\nu q^{-3}$

$H(1, \beta) = 1$; for $x_1 \geq 2$: $H(x_1, \beta) \approx \frac{3}{2\beta+3} x_1^{2\beta}$

Emission measure visible part isothermal wind (without contribution from cone obscured by the star):

$$EM = \int_{V_{\rm vis}} n_{\rm e} n_{\rm i} d^3\mathbf{r} = \gamma \int_{V_{\rm vis}} n_{\rm i}^2 d^3\mathbf{r} \equiv EM_0 P(x_1, \beta)$$

$$EM_0 = 2\pi\gamma R_*^3 \left(\frac{\dot{M}}{4\pi R_*^2 v_\infty \mu m_{\rm H}} \right)^2 = 1.1\ 10^{53} F_{\rm R,13}^{3/2} \frac{1}{\overline{G_{\rm ff,R}}} \left(\frac{R_*}{R_\odot} \right)^{-1} = 8.1\ 10^{52} \left(\frac{\dot{M}_{-10}}{v_{\infty,7}} \right)^2 \left(\frac{R_*}{R_\odot} \right)^{-1} \frac{\gamma}{\mu^2}\ {\rm cm}^{-3}$$

$$P(x_1, \beta) \equiv \frac{x_1^{2\beta}}{2\beta+1} \left(1 - x_1^{-2\beta-1}\right) + \frac{1}{x_1} + \frac{1}{2} x_1^{2\beta} \left(B(\beta + \tfrac{1}{2}, \tfrac{3}{2}) - B_{1/x_1^2}(\beta + \tfrac{1}{2}, \tfrac{3}{2}) \right) + \frac{1}{2} B_{1/x_1^2}(\tfrac{1}{2}, \tfrac{3}{2})$$

$P(1, \beta) = 1 + \pi/4$; for $x_1 \geq 2$: $P(x_1, \beta) \approx x_1^{2\beta} \left(\frac{1}{2\beta+1} + \frac{1}{2} B(\beta + \frac{1}{2}, \frac{3}{2}) \right)$

Neutral hydrogen column density:

$$N_{\rm H} = \int_{R_*}^\infty n(H\ I) dr = \zeta \int_{R_*}^\infty n_{\rm H} dr = \frac{\zeta}{S_{\rm i}} \int_{R_*}^\infty n_{\rm i} dr \equiv N_0 \left\{ \frac{1}{x_1} + \frac{x_1^\beta}{\beta+1} \left(1 - x_1^{-\beta-1}\right) \right\}$$

$$N_0 = R_* \left(\frac{\dot{M}}{4\pi R_*^2 v_\infty \mu m_{\rm H}} \right) \frac{\zeta}{S_{\rm i}} = 4.3\ 10^{20} \left(\frac{R_*}{R_\odot} \right)^{-1} \frac{\dot{M}_{-10}}{v_{\infty,7}} \frac{\zeta}{\mu S_{\rm i}} = 5\ 10^{20} \left(\frac{R_*}{R_\odot} \right)^{-1} F_{\rm R,13}^{3/4} (\overline{G_{\rm ff,R}}\gamma)^{-1/2} \frac{\zeta}{S_{\rm i}}\ {\rm cm}^{-2}$$

Effective radius $x_{\rm eff} = r_{\rm eff}/R_*$:

$x_{\rm eff} > x_1$ $\quad x_{\rm eff} = X_* X_\nu B_{\rm w} (4\pi R_*)^2 / F_\nu$

$x_{\rm eff} < x_1$ $\quad F_\nu = X_* X_\nu B_{\rm w} (4\pi R_*)^2 \left\{ \frac{1}{x_1} + \frac{x_1^{2\beta}}{2\beta+1} \left(x_{\rm eff}^{-2\beta-1} - x_1^{-2\beta-1} \right) \right\}$

at radio frequencies $x_{\rm eff} \gg x_1$: $x_{\rm eff} = 4 (X_* X_\nu)^{1/3} (\pi/2)^{-2/3} / \Gamma(\frac{1}{3})$

Effective optical depth $\tau_{\rm eff}$:

$x_{\rm eff} > x_1$ $\quad \tau_{\rm eff} = \frac{1}{3} X_* X_\nu x_{\rm eff}^{-3}$

$x_{\rm eff} < x_1$ $\quad \tau_{\rm eff} = \frac{X_* X_\nu}{2\beta+3} x_1^{2\beta} \left\{ x_{\rm eff}^{-2\beta-3} - x_1^{-2\beta-3} \right\}$

at radio frequencies $x_{\rm eff} \gg x_1$: $\tau_{\rm eff} = \frac{1}{3} X_* X_\nu x_{\rm eff}^{-3} = 0.2471$

The total flux emitted by the star and the wind is easily calculated following the standard procedure outlined by Wright and Barlow (1975), Panagia and Felli (1975) and Lamers and Waters (1984). The total flux $F_\nu = 4\pi d^2 f_\nu$ is given by

$$F_\nu = 8\pi^2 R_*^2 \int_0^1 B_* {\rm e}^{-\tau_{max}(q)}\, q dq + 8\pi^2 R_*^2 \int_0^\infty B_{\rm w} \left(1 - {\rm e}^{-\tau_{max}(q)}\right) q dq \qquad (10)$$

where $B_* = B(\nu, T_*)$, $B_{\rm w} = B(\nu, T_{\rm w})$, $B(\nu, T)$ is the Planck function, T_* is the black-body temperature of the star, $T_{\rm w}$ is the wind temperature and q is the impact parameter of the line of sight (see e.g. Fig. 1 in Lamers and Waters, 1984). The optical

depth at impact parameter q is given by

$$q > 1: \ \tau_{\max}(q) = 2\int_q^\infty \frac{X_* X_\nu}{w^2 x^3 \sqrt{x^2-q^2}} dx$$
$$q \leq 1: \ \tau_{\max}(q) = \int_1^\infty \frac{X_* X_\nu}{w^2 x^3 \sqrt{x^2-q^2}} dx$$

The optical depth depends of course on the assumed velocity law of the wind for which no information is available from observations. Therefore we use in this paper a velocity law for a wind which is accelerating up to some distance R_1 and then obtains its final velocity v_∞

$$v(r) = v_0(r/R_*)^\beta \ \text{ for } \ r < R_1; \ v(r) = v_\infty \ \text{ for } \ r \geq R_1 \ .$$

The acceleration of the wind is determined by the value of β. The dimensionless velocity is given by $w = (x/x_1)^\beta$ for $x < x_1$ and $w = 1$ for $x \geq 1$.

Given a velocity law for the wind, the run of the ion density in the wind $n_{\rm i}(r)$ can be determined from Eq. (1). In Table 2 the related expressions for $\tau_{\max}(q)$ are listed. Also listed in Table 2 are the expressions for the emission measure EM of the wind and the neutral hydrogen column density $N_{\rm H}$ along the line of sight at the centre of the star. For the emission measure we took into account that part of the wind does not contribute since it is obscured by the star.

With the expressions for $\tau_{\max}(q)$, as given in Table 2, part of Eq. (10) can be evaluated analytically resulting in

$$\begin{aligned}\frac{F_\nu}{8\pi^2 R_*^2} &= \int_0^1 B_* \mathrm{e}^{-\tau_{max}(q)}\, q dq + \int_0^1 B_{\rm w}\left(1-\mathrm{e}^{-\tau_{max}(q)}\right) q dq \\ &+ \int_1^{x_1} B_{\rm w}\left(1-\mathrm{e}^{-\tau_{max}(q)}\right) q dq \\ &+ B_{\rm w}\frac{1}{2}x_1^2\left\{\mathrm{e}^{-V} - 1 + V^{2/3}\gamma(\frac{1}{3},V)\right\} \end{aligned} \quad (11)$$

with $V = (\pi/2)X_* X_\nu / x_1^3$ and $\gamma(a,x)$ the incomplete Gamma function (Abramowitz and Stegun, 1968). The first term on the right accounts for the emission by the star, which can be attenuated by absorption due to the wind. The second term accounts for the emission from the cone in front of the star while the third term accounts for the emission from the wind acceleration region outside the previously mentioned cone. The fourth term described the emission from the volume (outside the cone) where the wind has reached its terminal velocity. Note that for a wind with constant velocity ($x_1 = 1$) the third term does not contribute. At low frequencies, at which τ is large, only the last term effectively contributes to the flux resulting in

$$\begin{aligned} F_\nu &= 4\pi^2 R_*^2 B_{\rm w}\Gamma(\frac{1}{3})\left(\frac{1}{2}\pi X_* X_\nu\right)^{2/3} \\ &= 5.14\ 10^{-6}\left(\frac{\gamma}{\mu^2}\right)^{2/3}\left(\frac{\dot{M}}{v_\infty}\right)^{4/3}(\overline{G_{\rm ff}}\nu)^{2/3} \end{aligned} \quad (12)$$

which is identical to the expression found by Wright and Barlow (1975). At higher frequencies, at which τ becomes small, we can make the approximation $1 - \exp(-\tau_{\max}(q)) \approx \tau_{\max}(q)$ in Eqs. (10) and (11). Evaluation of the resulting integrals shows that, at frequencies at which the emission is optically thin, the flux is given by

$$\begin{aligned} F_\nu &= 4\pi^2 R_*^2 B_* + 8\pi^2 R_*^2 B_{\rm w} X_* X_\nu P(x_1,\beta) \\ &= 4\pi^2 R_*^2 B_* + EM\epsilon(\nu,T) \end{aligned} \quad (13)$$

with $P(x_1,\beta)$ given in Table 2 and $\epsilon(\nu,T)$ the free-free emissivity (e.g. Rybicki and Lightman, 1979)

$$\epsilon(\nu,T) = \frac{6.8\ 10^{-38}}{T^{1/2}}\exp\left(\frac{-h\nu}{kT}\right)\overline{G_{\rm ff}}\ \text{erg s}^{-1}\text{cm}^3\text{Hz}^{-1} \ . \quad (14)$$

The last identity in Eq. (13) results from applying Kirchhoff's law. As could be anticipated, in the optically thin part of the spectrum the flux is composed of the contribution by the star and the free-free emission from a wind with an emission measure EM.

For completeness we present in Table 2 also the effective radius $r_{\rm eff}$ and the effective optical depth $\tau_{\rm eff}$ (see Wright and Barlow, 1975). The effective radius is defined by assuming that the emission at a given frequency originates from the volume at $r > r_{\rm eff}$

$$F_\nu = \int_{r_{\rm eff}}^\infty (4\pi)^2 B_{\rm w}(\nu,T_{\rm w})\kappa(\nu,T_{\rm w})r^2 dr$$

with F_ν given by Eq. (10). The effective optical depth is then defined by $\tau_{\rm eff} = \int_{r_{\rm eff}}^\infty \kappa(\nu,T_{\rm w})dr$.

3. Applications to observations

Fig. 1 shows that the flux distributions of the three objects are very similar. Therefore we start with a discussion of the flux distributions in general terms before turning to the specific objects. From the observed flux at radio frequencies (Eq. (12)) it follows that

$$\frac{\dot{M}_{-10}}{v_{\infty,7}} = 1.17\mu F_{\rm R,13}^{3/4}(\overline{G_{\rm ff,R}}\gamma)^{-1/2} \quad (15)$$

where $\dot{M}_{-10}$ is the mass loss rate in units of 10^{-10} $\mathrm{M}_\odot$/yr, $v_{\infty,7}$ is the terminal wind velocity in units of 100 km/s, $F_{\rm R,13}$ is the observed flux at 6 cm ($\log\nu = 9.7$) in units of 10^{13} erg s^{-1}Hz^{-1}. $\overline{G_{\rm ff,R}}$ is the gaunt factor at $\log\nu = 9.7$ as given in Table 1. Because for all objects $F_{\rm R,13}$ is of the order unity, Eq. (15) shows that the radio fluxes imply mass loss rates of the order of 10^{-10} $\mathrm{M}_\odot$/yr as was inferred by MDRM who took $v_{\infty,7} \approx 3$. Also it follows that the wind temperature has to be higher than 10^4 K because otherwise μ is so large (see Table 1) that unrealistic mass loss rates ($> 10^{-8}$ $\mathrm{M}_\odot$/yr) result.

An important assumption made by MDRM is that the observed power-law distribution $F_\nu \sim \nu^\alpha$ in the radio – IR frequency range is indicative of a stellar wind. This assumption is based on the fact that similar power-laws are observed for early type stars loosing mass. There is however an important difference between the above inferred mass loss rate for dMe

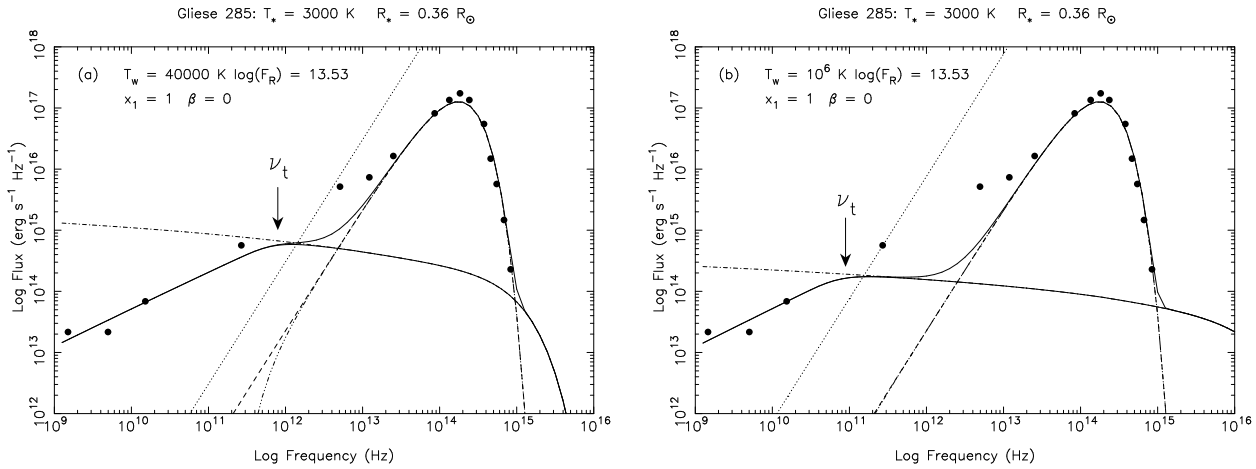

Fig. 3a and b. Flux distributions for constant velocity winds with temperatures of **a** $T_{\rm w}$ = 4 10^4 K and **b** $T_{\rm w}$ = 10^6 K. The dots are the observed fluxes for YZ CMi (Fig. 1a). The thick solid line is the resulting distribution from the wind and the star (Eq. (11)). The thin solid line is the contribution by the wind which dominates at low frequencies. The dashed-triple dot line is the contribution by the star (first term in Eq. (11)). The dashed line is the black-body curve for the star and the dotted line that for the wind. For these curves the area is taken equal to the stellar disk. The dashed-dotted line is the optically thin approximation (Eq. (13)) which is very accurate at frequencies above the frequency $\nu_{\rm t}$.

stars and that of early type stars. The latter have mass loss rates in the range $10^{-5} - 10^{-8}$ $M_\odot$/yr which is a factor $10^2 - 10^5$ larger than the data for dMe stars suggest. This has important consequences for the flux distribution because the lower mass loss rates of dMe stars will result in smaller optical depths. This leads to a modification of the spectrum and in the following we show that, if dMe stars loose mass at a rate of 10^{-10} $M_\odot$/yr, the resulting flux distribution is not a power-law in the radio – IR range. Apart from the fact that the optical depths in the winds differ, there is a second difference between early and late type stars: for early type stars $T_* > T_{\rm w}$ while for dMe stars the reverse holds.

Because $h\nu/kT$ = 1 occurs at frequency ν = 2 $10^{14} T_4$ Hz we can use for $B_{\rm w}$ and B_* the Rayleigh-Jeans approximation while in Eq. (9) $X_\nu \approx \nu^{-2}\overline{G_{\rm ff,R}}$. From Eqs. (8) and (15) it follows that

$$X_* = 6.4\ 10^{22} F_{\rm R,13}^{3/2} T_4^{-3/2} \left(\frac{R_*}{R_\odot}\right)^{-3} \frac{1}{\overline{G_{\rm ff,R}}}$$
$$= 4.7\ 10^{22} \left(\frac{\dot{M}_{-10}}{v_{\infty,7}}\right)^2 T_4^{-3/2} \left(\frac{R_*}{R_\odot}\right)^{-3} \frac{\gamma}{\mu^2} \qquad (16)$$

In order to discuss the flux distribution it is useful to consider the optical depth along the line of sight passing through the center of the star $\tau_{\rm max}(0)$. Cassineli et al. (1977) have argued that the emission originates from τ = 1/3. It is convenient to introduce the optical depth $\tau_0 = X_* X_\nu H(x_1, \beta)$ with H defined in Table 2. At some frequency $\nu_{\rm t}$, τ_0 will become unity. Because $\tau_0 \sim X_\nu \sim \nu^{-2}$, the transition between optically thick and optically thin will occur rapidly near this frequency. Unit optical depth corresponds to $X_* X_\nu H$ = 1 or

$$\nu_{\rm t} = 2.54\ 10^{11} \sqrt{H} \left(\frac{F_{\rm R,13} R_\odot^2}{T_4 R_*^2}\right)^{3/4} \left(\frac{\overline{G_{\rm ff}}(\nu_{\rm t}, T)}{\overline{G_{\rm ff,R}}}\right)^{1/2} \text{Hz}. \qquad (17)$$

Table 3. The values for ν_{x_1}, $\nu_{\rm t}$ and ν_1 for the models shown in Fig. 4.

no.	x_1	β	$\nu_{11}(x_{\rm eff} = x_1)$	$\nu_{\rm t,11}$	$\nu_{12}(x_{\rm eff} = 1)$
1	1	0	19.9	7.9	1.99
2	2	0.5	3.4	9.6	2.43
3	2	1	3.4	10.3	3.04
4	2	5	3.3	98.5	27.66
5	5	0.5	0.9	14.5	3.68
6	5	1	0.9	27.7	7.05

For x_1 = 1 (constant velocity wind) H = 1. At frequencies below $\nu_{\rm t}$ the wind is optically thick and has a $F_\nu \sim (\overline{G_{\rm ff}}\nu)^{2/3}$ spectral distribution while at higher frequencies the optically thin approximation Eq. (13) applies. Eq. (13) shows that, in the optically thin part of the spectrum, the contribution by the wind is almost independent of frequency, at frequencies $h\nu < kT_{\rm w}$, apart from a small variation caused by the frequency dependence of the gaunt factor. We define $\nu_{\rm th} \equiv kT_{\rm w}/h$. At $\nu > \nu_{\rm th}$ the wind emission drops rapidly as $\exp(-h\nu/kT_{\rm w})$.

In Fig. 3 we show the calculated emission from the star and the wind (for x_1 = 1) as follows from numerical integration of Eq. (11) for $T_{\rm w}$ = 4 10^4 K and $T_{\rm w}$ = 10^6 K (thick solid lines). Also indicated are the black-body distributions from the star and the wind, the separate contributions by the star and the wind to the observed flux and the optically thin approximation (Eq. 13). The data points for YZ CMi are also plotted. The figures clearly show that up to frequency $\nu_{\rm t}$ the flux distribution is that of a mass loosing star, as assumed by MDRM, but at frequency $\nu_{\rm t}$ the wind contribution becomes relatively flat. At higher frequencies the contribution by the star starts to dominate the spectrum. In the range $\nu_{\rm t} < \nu < \nu_{\rm th}$ the variation of the wind contribution is only

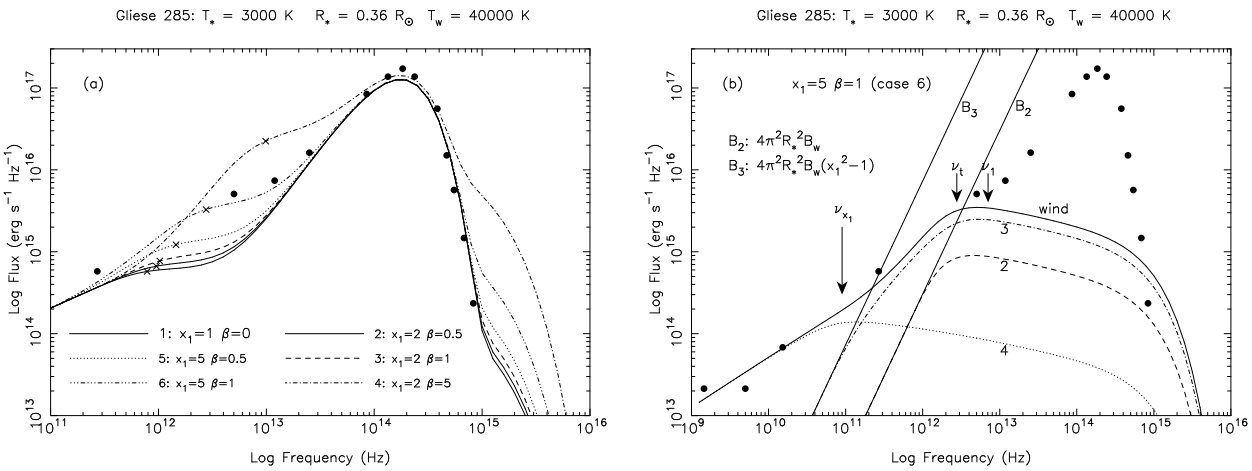

Fig. 4. a Flux distributions for six combinations of x_1 and β and a wind temperature of $T_{\rm w}$ = 4 10^4 K. The data points are those for YZ CMi. Case 1 corresponds to Fig. 3a. **b** Contributions to the total wind emission for case 6 in panel (a). The solid curve is the total emission from the wind. The curves labeled 2, 3 and 4 correspond to the second, third and fourth term on the left hand side of Eq. (11). Curve B_2 is the flux from a black-body with a area equal to the stellar disk. Curve B_3 is the flux from a black-body with a area equal to the acceleration region minus the stellar disk area. At frequency ν_{x_1} the effective radius equals the size of acceleration region. At frequency $\nu_{\rm t}$ the emission becomes optically thin and at frequency ν_1 the effective radius equals the stellar radius.

caused by the gaunt factor. In Fig. 3a frequency $\nu_{\rm th}$ corresponds to 8 10^{14} Hz above which frequency the wind contribution drops exponentially. Note that at frequencies $> \nu_{\rm t}$ the optically thin approximation (Eq. 13) is very accurate. For low temperatures of the wind, like e.g. 4 10^4 K, the black-body emission by the star is slightly reduced due to wind absorption but at those frequencies the wind emission dominates anyway. Figs. 3a and 3b show that frequency $\nu_{\rm t}$ goes up as the temperature of the wind increases. Because $\nu_{\rm t} \sim T^{-3/4}$, apart from a weak dependence on the Gaunt factor, reducing the wind temperature to a value lower than 4 10^4 K, like e.g. 1.5 10^4 K, does not improve the fit to the data points. The reason is that at frequency $\nu_{\rm t}$ the black body emission of the wind varies as $B_{\rm w} \sim \nu_{\rm t}^2 T_{\rm w} \sim T_{\rm w}^{-1/2}$ and is therefore only weakly dependent on the wind temperature. At the same time, for higher values of $\nu_{\rm t}$, the effective radius of the source $r_{\rm eff}$ becomes smaller. Together these effects result in that the flux distributions of winds with $T_{\rm w} < 4\ 10^4$ K resemble very much the flux distribution shown in Fig. 3a. We conclude that the observed flux distribution cannot be reconciled with that of a stellar wind because the *IRAS*- and, depending on the wind temperature, also the *JCMT*-data points are not fitted at all.

A possible way out would be to increase the optical depth so that $\nu_{\rm t}$ is found at IR frequencies. This can be accomplished by allowing the wind to accelerate over some distance (so increasing H in Eq. (17)). Fig. 3 shows that $\nu_{\rm t}$ has to be increased by at least a factor 100 in order to have the turn-over frequency near the *IRAS* points and that cool winds are preferable. Eq. (17) and Table 2 show that $\nu_{\rm t} \sim \sqrt{H} \sim x_1^{\beta}\sqrt{3/(2\beta+3)}$. Therefore either x_1 or β has to be large, or both. This has however a strong effect on the emission measure which scales as $EM \sim P \sim x_1^{2\beta}(1/(2\beta+1) + 0.5B(\beta+0.5, 1.5))$. The strong increase of the emission measure which occurs when the wind is allowed to accelerate has a dramatic effect on the flux distribution at high frequencies. To illustrate this we show in Fig. 4a the flux distributions for six combinations of the parameters x_1 and β. For each combination we give in Table 3 the values of the frequencies at which the emission becomes optically thin ($\nu_{\rm t}$), at which the effective radius equals the acceleration region (ν_{x_1} at $x_{\rm eff} = x_1$) and at which the effective radius equals the radius of the star (ν_1 at $x_{\rm eff} = 1$). The combination $x_1 = 1$, $\beta = 0$ (case 1) corresponds to the example given in Fig. 3a. In cases 2 - 4 we have kept the acceleration radius at two stellar radii and varied β while for cases 5 and 6 the acceleration radius is at five stellar radii.

The figure clearly shows that as $\nu_{\rm t}$ becomes higher the emission measure increases. This results in a (strong) increase of the flux at high frequencies. For all combinations of x_1 and β either the IR data points are not fitted or there is too much flux at frequencies above 10^{15} Hz. The flux distributions can be explained by considering the contributions by the different terms in Eq. (11). Because the *IRAS* data points are best fitted when $x_1 = 5$ and $\beta = 1$ we show in Fig. 4b the contributions by the different terms in Eq. (11) as an illustration. We start with the last term in Eq. (11) (curve 4 in Fig. 4b) which dominates at low frequencies and results in a $F_\nu \sim (\overline{G_{\rm ff}}\nu)^{2/3}$ distribution. The part in the curly brackets can be approximated as $\Gamma(1/3)V^{2/3}$ for $V > 5$ and as $2V$ for $V \lesssim 5$. This implies that near $V = 5$ the contribution by this term will change. $V = 5$ corresponds to $X_* X_\nu = (10/\pi)x_1^3 = 3.18x_1^3$. The frequency at which the effective radius equals the acceleration radius ($x_{\rm eff} = x_1$, see Table 2) corresponds to $X_* X_{\nu_{x_1}} \approx (\Gamma(1/3)/4)^3(\pi/2)^2 x_1^3 = 0.74x_1^3$. Combining these expressions we see that $V = 5$ corresponds to a frequency $\sqrt{0.74/3.18}\nu_{x_1} \approx 0.5\nu_{x_1}$. Above this frequency the contribution by the last term in Eq. (11) becomes flatter and

becomes proportional to $B_w x_1^2 V = (\pi/2) B_w X_* X_\nu / x_1$. This shows that for larger values of x_1 this term becomes relatively smaller at high frequencies. The flattening of the contribution above frequency $0.5\nu_{x_1}$ is clearly visible in curve 4 in Fig. 4b.

The second and third term of Eq. (11) are shown as curves 2 and 3 in Fig. 4b. At low frequencies, at which the emission is optically thick, these terms equal $0.5B_w$ and $0.5B_w(x_1^2 - 1)$ respectively. Their sum equals the flux from a black-body at temperature T_w and with a surface area set by the size of the acceleration region. Above frequency ν_{x_1} the outer parts of the acceleration region become increasingly optically thin. This has the effect that towards higher frequencies one observes the flux from a black-body B_w with a decreasing surface area (curve 3). At frequency ν_t the emission becomes optically thin. This occurs before frequency ν_1 (at which $r_{eff} = R_*$) is reached. In the frequency range $\nu_{x_1} \lesssim \nu < \nu_t$ the second and third term in Eq. (11) dominate. Because at these frequencies the flux is proportional to B_w, with $T_w > T_*$, the flux can become relatively strong (cases 4 and 6 in Fig. 4a). Table 3 shows that in the consecutive cases 2, 3, 5, 6 and 4 the difference between ν_{x_1} and ν_t becomes larger. Fig. 4a shows that larger differences between these frequencies are accompanied by stronger emission. The reason is that we have $T_w > T_*$ contrary to the situation in winds near early type stars.

The arguments used by MDRM to explain the power-law distributions shown in Fig. 1 were based on the theory for stellar winds from early type stars. Above we demonstrated that this theory cannot be applied to the (possible) winds of late type stars. The two fundamental differences are: 1) the derived mass loss rates for dMe stars from the radio data are factors $10^2 - -10^5$ smaller than for early type stars. This implies that the frequency at which the emission becomes optically thin ($\tau \sim X_* X_\nu \sim (\dot{M}/\nu)^2$), and the frequency at which $r_{eff} = R_1$, are found at lower frequencies. This results in a deviation from the power-law spectrum. MDRM assumed the presence of a power-law distribution between the radio and IR data points. 2) the winds in dMe stars are characterized by $T_w > T_*$. This has the consequence that at IR frequencies the emission can become very strong. Even more important is the fact that $T_w > T_*$ results in strong emission from the wind in the Wien part of the stellar black-body distribution. Although the flux distributions in the radio - IR range can be fitted by assuming the presence of a wind acceleration region, these models predict too much flux at frequencies $\nu \gtrsim 10^{15}$ Hz.

4. Alternative constraints

From the discussion in the previous section it must be concluded that it is unlikely that dMe stars loose mass at rates of 10^{-10} $M_\odot$/yr. If the mass loss rate is in reality lower, then the radio, *JCMT* and *IRAS* data points require alternative explanations. For the radio data these are readily available. The common interpretation of radio emission from dMe stars is gyro-synchrotron emission from non-thermal particles (or coherent emission). This interpretation is supported by the results of Benz and Alef (1991) who discuss intercontinental *VLBI* observations of YZ CMi at 1.7 GHz. They found that the source was not resolved at this frequency and found a radio diameter of 1.0 ± 0.5 mas or $1.7R_*$. The derived brightness temperature was $1.7\ 10^9$ K with a lower limit of $4\ 10^8$ K. This brightness temperature already rules out the possibility that the radio emission is caused by a stellar wind. If YZ CMi would be loosing mass at a rate of $\sim 10^{-10}$ $M_\odot$/yr, as suggested by MDRM, then the effective radius at 1.7 GHz would amount to

$$x_{eff} = \frac{r_{eff}}{R_*} = 133 \left(\frac{\dot{M}_{-10}}{v_{\infty,7}}\right)^{2/3} T_4^{-1/2} \left(\frac{\gamma}{\mu^2}\right)^{1/3} \left(\frac{g_{1.7}}{5}\right)^{1/3}$$

with $g_{1.7}$ the gaunt factor at 1.7 GHz. A source of this size would certainly have been resolved with intercontinental *VLBI*. Alternatively, we can argue that at 1.7 GHz r_{eff} has to be smaller than the $1.7R_*$ found by Benz and Alef. This gives an upper limit for the mass loss rate which is compatible with the VLBI results

$$\frac{\dot{M}_{-10}}{v_{\infty,7}} < 1.4\ 10^{-3} T_4^{3/4} \left(\frac{\mu^2}{\gamma}\right)^{1/2} \left(\frac{g_{1.7}}{5}\right)^{-1/2} . \quad (18)$$

This upper limit automatically implies that the wind is optically thin at radio frequencies. The frequently observed nonthermal emission from dMe stars implies that this emission is not absorped by a wind. Requiring that the optical depth of the wind at e.g. 6 cm is less than unity gives

$$\frac{\dot{M}_{-10}}{v_{\infty,7}} < 2.2\ 10^{-3} T_4^{3/4} \left(\frac{\mu^2}{\gamma}\right)^{1/2} \left(\frac{g_5}{5}\right)^{-1/2} . \quad (19)$$

with g_5 the gaunt factor at 5 GHz. Comparing Eqs. (18) and (19) shows that they have the same form but that the upper limit set by the *VLBI* observations is slightly more restrictive.

Additional constraints on the mass loss rate can be obtained by considering the observed fluxes at other frequencies. E.g. from the data presented by Doyle (1989) it follows that the flux from YZ CMi in the *IUE–SWP* band-pass (1150 − 1950 Å) amounts to $\log F_{IUE} = 28$ (in erg s^{-1}). Güdel et al. (1993) give for the flux in the *ROSAT–PSPC* band-pass (0.1 − 2.4 keV) a flux of $\log F_{Rosat} = 28.47$. We have calculated the emissivities in these band-passes for the temperatures listed in Table 1 using the Utrecht spectral code SPEX (Kaastra and Mewe, 1993, Mewe and Kaastra, 1994). From the fact that any emission from a stellar wind must not exceed the observed fluxes, a maximum value for the permitted emission measure can be derived. By using the expression for EM, as given in Table 2, this can be translated into an upper limit for $\dot{M}/v_\infty$. Another constraint follows from the fact that the wind must not contribute substantially to the interstellar absorption between the star and the observer. There have been no reports that spectral fits of EUV and X-ray data from dMe stars require abnormal column densities. Interstellar absorption is caused by photo-ionization. In the expression for the neutral hydrogen column density given in Table 2 we have only considered the presence of hydrogen. In that way the expression for N_H yields only an lower limit to the absorption by a wind. By assuming that the absorption by

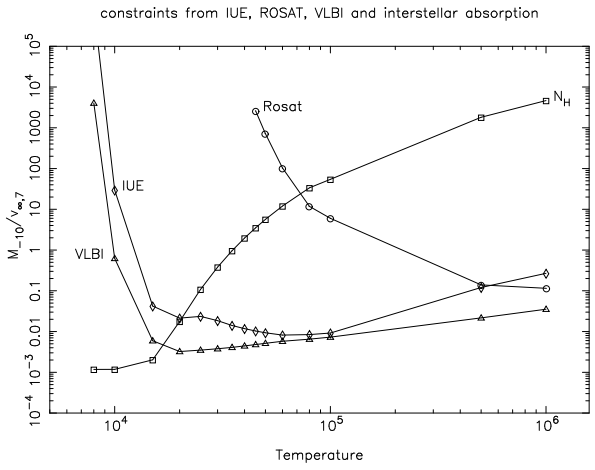

Fig. 5. Constraints on the mass loss rate of YZ CMi as follow from the maximum source size set by $VLBI$ observations, the observed fluxes in the $IUE - SWP$ and the $ROSAT - PSPC$, and the constraint that the neutral hydrogen column density in the wind must be smaller than 10^{18} cm^{-2}. The horizontal axis corresponds to the temperature of the wind. Each curve corresponds to the upper limit for $\dot{M}_{-10}/v_{\infty,7}$ as follows from a specific instrument or constraint. All curves are for winds with constant velocities ($x_1 = 1$). At each temperature the lowest curve presents the relevant constraint.

the wind must not exceed the canonical value $N_{\rm H} = 10^{18}$ cm^{-2} an additional constraint for $\dot{M}/v_\infty$ follows.

In Fig. 5 we show the upper limits for $\dot{M}/v_\infty$ as follow from 1) $VLBI$ (Eq. (18)), 2) the neutral hydrogen absorption $N_{\rm H}$, 3) the observed flux in the $IUE - SWP$ band-pass and 4) the observed flux in the $ROSAT - PSPC$ band-pass. It is important to emphasize that each curve, related to a specific instrument, provides the best constraint in a specific temperature range, e.g. for a hot stellar wind ($\sim 10^6$ K) the neutral hydrogen column density would be a rather poor constraint; in this case it is better to use the radio and/or X-ray data. At 10^5 K IUE and $VLBI$ provide good constraints. The figure shows that, as expected, at low temperatures (< 17.000 K) the neutral hydrogen absorption provides the most stringent constraint. The upper limit for the $VLBI$ source size gives the most important constraint while IUE and $ROSAT$ also provide reasonably useful constraints. Note that the latter constraints were derived assuming that the emission by the wind equals at most the observed flux. If one were to use as a constraint that the allowable wind emission is only a fraction f of the observed flux (in order not to mask the coronal emission), then the IUE and $ROSAT$ curves in Fig. 5 must be multiplied by a factor $\sqrt{f}$.

All curves in Fig 5 are calculated for winds without an acceleration region ($x_1 = 1$). The constraints set by the IUE and $ROSAT$ fluxes are proportional $1/\sqrt{P(x_1,\beta)} \sim 1/x_1^\beta$ so that the presence of an acceleration region near the star can considerably reduce the upper limits for the mass loss shown in the figure. The same applies for the constraint set by the neutral hydrogen column density which (roughly) scales with $(\beta+1)/x_1^\beta$. Furthermore, all curves are for a terminal wind velocity of 100 km/s. Higher velocities of the wind lead to a proportionally higher vlaue for the allowable mass loss rate.

At low temperatures a large number of atoms in the wind is not fully ionized. Therefore the permitted value for the mass loss rate at temperatures $\lesssim 3\ 10^4$ K is likely to be at least a factor two lower than indicated in the figure because we did not consider the presence of He, C, N and O in the expression for $N_{\rm H}$. In-between the IUE and $ROSAT$ curves, data from the Extreme Ultraviolet Explorer $EUVE$ can probably result in additional constraints given the wavelength range covered by the $EUVE$. For YZ CMi no $EUVE$ data are however available to us. Also more refined constraints can be obtained by considering the observed fluxes from individual lines in e.g. IUE spectra. For the moment we conclude that if the wind temperature is in the range $2\ 10^4 \leq T_{\rm w} \leq 10^5$ K, the mass loss rates of dMe stars must be $\lesssim 10^{-12}$ M$_\odot$/yr. At higher temperatures a safe upper limit is $2\ 10^{-12}$ M$_\odot$/yr. At these rates the winds will not result in an observable signal in the radio – IR range. Because the frequency at which the spectrum becomes optically thin is proportional to the mass loss rate, $\nu_{\rm t}$ will be at least a factor 100 lower than the values given in Table 3. At radio frequencies the flux by the wind is reduced by at least a factor $10^{8/3} = 464$ (Eq. (12)).

The only way to infer the presence of such tenuous winds is by considering the effect the wind has on the strength of strong spectral lines at EUV wavelengths. Schrijver et al. (1994) pointed out that strong lines can be subject to resonant scattering. Although scattering does not result in photon destruction, except in the case of branching, these authors demonstrated that, if an asymmetry is introduced between the emitting volume and the scattering volume, the photon flux towards the star can be increased. The photons can then be destroyed at the stellar surface. In the case of a chromosphere/corona embedded in a stellar wind the required asymmetry follows naturally. The photons emitted in the chromosphere or corona are then scattered in the tenuous wind and a fraction is subsequently destroyed upon impact at the stellar surface. Weak lines are not affected by scattering and therefore this effect can lead to a detectable difference between the ratio of line intensities of weak and strong lines and the expected ratio. The optical depth (at the line centre) for scattering is given by

$$\tau = 10^{-19} C_{\rm d} \left(\frac{A_{\rm Z}}{A_{\rm Z,\odot}}\right) \frac{n_{\rm e}\ell}{\sqrt{T_6}}\ .$$

The constants $C_{\rm d}$ can be found in Schrijver et al. for a number of strong lines. In general their values are in the range $0.5 \lesssim C_{\rm d} \lesssim 2$. The electron column density of the scattering medium is given by $n_{\rm e}\ell$. In the case of a stellar wind we have

$$n_{\rm e}\ell = 4.3\ 10^{18} \frac{\gamma}{\mu} \left(\frac{R_*}{R_\odot}\right)^{-1} \frac{\dot{M}_{-12}}{v_{\infty,7}} = 1.2\ 10^{19} \frac{\gamma}{\mu} \frac{\dot{M}_{-12}}{v_{\infty,7}}$$

where the last step applies to YZ CMi. These expressions show that for mass loss rates of the order of 10^{-12} M$_\odot$/yr the optical depth for scattering can become unity leading to a detectable effect. On the other hand it can be argued that if the mass loss

rate would be of the order of 10^{-10} $M_\odot$/yr, the optical depth for resonant scattering would be $\sim$ 100. This would have a dramatic effect on the strong lines in EUV and X-ray spectra which would be strongly attenuated. There is no observational evidence that this occurs. An illustration of the effect of photon scattering, for inferring the presence of a tenuous wind from Procyon, can be found in Schrijver et al. (1996).

Finally we note that Fig. 5 is compiled under the assumption that the wind is isothermal and that the ionization balance reflects the kinetic temperature in the wind. If the temperature of the wind would drop with radial distance, while the ionization balance would be determined by a much higher freezing-in temperature, a different situation arises. In that case we would be dealing with a cool wind which is still e.g. fully ionized ('over-ionized'). This results in a modification of the *VLBI* constraint. The reason why the *VLBI* curve turns upward near 10^4 K is that at low temperatures the plasma contains many neutrals and μ becomes large in Eq. (18). If we would be dealing with a cool wind, which is over-ionized because of freezing-in at the base, then μ and γ in Eq. (18) must be evaluated at the much higher ionization temperature. Taking $\mu \approx 1.283$ and $\gamma \approx 1.09$ (see Table 1) changes the *VLBI* constraint to

$$\frac{\dot{M}_{-10}}{v_{\infty,7}} < 1.7\ 10^{-3} T_4^{3/4} \left(\frac{g_{1.7}}{5}\right)^{-1/2} \qquad (20)$$

with T now the kinetic temperature of the wind. This shows that for cool over-ionized winds the *VLBI* constraint almost coincides with the $N_{\rm H}$ curve at $T \leq 17.000$ K. Of course, when over-ionization due to a frozen-in ionization balance occurs the $N_{\rm H}$ curve is not relevant anymore because there are no neutrals. But at the same time the *VLBI* constraint becomes as restrictive as the original $N_{\rm H}$ constraint at low temperatures.

5. Conclusions

In this paper we have demonstrated that the observed power-law flux distributions of a number of dMe stars in the radio – IR frequency range cannot be reconciled with that of a stellar wind. Although the radio data suggest mass loss rates of the order of 10^{-10} $M_\odot$/yr, the resulting flux distribution is not a power-law. The reason is that this mass loss rate is much lower than the rates of hot stars leading to a reduction of the optical depths in the wind and a corresponding modification of the spectrum. A second difference is caused by the fact that for dMe stars the temperatures of the winds are higher than the effective temperatures of the stars. If the radio, *JCMT* and *IRAS* are to be fitted simultaneously, it is necessary to invoke the presence of a wind acceleration region. This increases the emission measure of the wind so strongly that at high frequencies $> 10^{15}$ Hz a strong excess is present which has not been observed. This excess is caused by the fact that the required emission measure is so high and that $T_{\rm w} > T_*$.

Reliable upper limits for the mass loss rate from dMe stars can be obtained by considering the fact that the flux by the wind must not exceed the *observed* fluxes by instruments like *IUE* and *ROSAT*. Also, at radio wavelengths the size of the wind region cannot exceed the upper limits for the radio source size as follow from intercontinental *VLBI*. Furthermore, if the winds are cool ($\lesssim 4\ 10^4$ K), the contribution to the interstellar absorption must not be larger than $\sim 10^{18}$ cm^{-2}. By applying these constraints we arrive at an upper limit for the mass loss rate of 10^{-12} $M_\odot$/yr. At higher temperatures, e.g. 10^6 K a safe upper limit is $2\ 10^{-12}$ $M_\odot$/yr. Additional support for this upper limit comes from the fact that at higher mass loss rates EUV and X-ray line photons would be subject to considerable scattering in the wind (and possibly subsequent photon destruction). This has not been observed.

Even if the mass loss from dMe stars would amount to 10^{-12} $M_\odot$/yr the observed excess fluxes at mm wavelengths and in the IR cannot be explained by a stellar wind. This implies that if instruments like *ISO* and *SCUBA* would find evidence of excess emission, alternative explanations, like e.g. emission from circumstellar dust, are required.

If the mass loss is to proceed in a clumpy way, in the form of coronal mass ejections, then our arguments still apply. If there are only a few remnants of ejecta around the star the approach we followed in this paper is not valid but then the contribution to a possible stellar wind is small anyway. If there are many ejecta near the star, then one has to consider the way this affects the optical depth $\tau_{\rm max}(q)$. In general it will be reduced compared to a homogeneous wind. This will cause the turn-over frequency $\nu_{\rm t}$ to shift to lower frequencies resulting in lower fluxes at mm and infrared wavelengths. If the number of ejecta becomes very high then one approaches the situation of a homogeneous wind as we considered in this paper.

Given the reduction of the maximum allowable mass loss rate from dMe stars by a factor 100, when compared to the estimates by MDRM, the winds from dMe stars become less important a mass donors for the interstellar medium. At most they contribute 0.1 $M_\odot$/yr but it is likely that as additional constraints from *EUVE* data and *VLBI* observations become available, this number will be reduced. Finally we note that our derived upper limits for the mass loss rate are in agreement with the (independently) derived upper limits by Lim and White (1996).

Acknowledgements. G.H.J. van den Oord acknowledges financial support from the Netherlands Organization for Scientific Research (NWO). Research at Armagh Observatory is grant-aided by the Dept. of Education for N. Ireland. We thank the referee for carefully reading the manuscript and for pointing out the necessity to consider over-ionized winds.

References

Abramowitz, M., Stegun, I.A. 1968, Handbook of Mathematical Functions, Dover Publications, New York
Allen, C.W. 1973, Astrophysical Quantities, Athlone Press, London
Anders, E., Grevesse, N. 1989, Geochimica et Cosmochimica Acta, 53, 197
Arnaud, M., Rothenflug, R. 1985, A&AS, 60, 425
Arnaud, M., Raymond, J.C. 1992, ApJ, 398, 394
Benz, A.O., Alef, W. 1991, A&A, 252, L19

Cassinelli, J.P., Hartmann, L. 1977, ApJ, 212, 488
Doyle, J.G. 1989, A&A, 214, 258
Doyle, J.G., Mathioudakis, M. 1991, A&A, 241, L41
Güdel, M., Schmitt, J.H.M.M., Bookbinder, J.A., Fleming, T.A. 1993, ApJ, 415, 236
Gronenschild, E.H.B.M., Mewe, R. 1978, A&AS, 32, 283
Houdebine, E.R., Foing, B.H., Rodonò, M. 1990, A&A, 238, 249
Kaastra, J.S., Mewe, R. 1993, Legacy, 3, 16
Lamers, H.J.G.L.M., Waters, L.B.F.M. 1984, A&A, 136, 37
Leitherer, C., Robert, C. 1991, ApJ, 377, 629
Lim, J., White, S.M. 1996, ApJ, 462, L91
Mewe, R., Lemen, J.R., van den Oord, G.H.J. 1986, A&AS, 65, 511
Mewe, R., Kaastra, J.S. 1994, European Astron. Soc. Newsletter, 8, 3
Mullan, D.J., Sion, E.M., Bruhweiler, F.C., Carpenter, K.G. 1989, ApJ, 339, L33
Mullan, D.J., Doyle, J.G., Redman, R.O., Mathioudakis, M. 1992, ApJ, 397, 225 (MDRM)
Panagia, N., Felli, M. 1975, A&A, 39, 1
Rybicki, G.B., Lightmann, A.P. 1979, Radiative Processes in Astrophysics, Wiley & Sons, New York
Schrijver, C., van den Oord, G.H.J., Mewe, R. 1994, A&A, 289, L23
Schrijver, C., van den Oord, G.H.J., Mewe, R., Kaastra, J.S. 1996, in Astrophysics in the Extreme Ultraviolet, S. Bowyer, R. Malina (eds.), p. 121, Kluwer
Waters, L.B.F.M., Lamers, H.J.G.L.M. 1984, A&AS, 57, 327
Wright, A.E., Barlow, M.J. 1975, MNRAS, 170, 41

This article was processed by the author using Springer-Verlag LaTeX A&A style file *L-AA* version 3.